Ecological Engineering 233 (2026) 108145

Contents lists available at ScienceDirect

Ecological Engineering

journal homepage: www.elsevier.com/locate/ecoleng

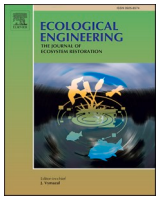

Lowering a navigation groyne increases the frequency of flooding and reduces greenhouse gas evasion from an oxbow lake

Sara Benelli, Bianca Maria Lecchini, Marco Bartoli *

Department of Chemistry, Life Sciences and Environmental Sustainability, University of Parma, Parco Area delle Scienze 33/A, 43124 Parma, Italy

ARTICLE INFO

Keywords:
River restoration
River-floodplain connectivity
Greenhouse gas fluxes
Greenhouse gas saturation
Agricultural nutrient loading

ABSTRACT

Lowering navigation groynes can restore lateral connectivity between regulated rivers and adjacent floodplains. In the Po River, northern Italy, this intervention increased the frequency of hydraulic connection between the river and the Gussola oxbow lake. However, despite the potential effects of reconnection on oxygen conditions, nutrient supply, organic matter processing and biodiversity, little is known about how alternating periods of connection and disconnection regulate greenhouse gas (GHG) emissions from oxbow lakes. Carbon dioxide (CO_2), methane (CH_4), and nitrous oxide (N_2O) saturation and fluxes, and water physical-chemical parameters, were measured for one year at the Gussola oxbow lake, periodically connected to the Po River. We hypothesized that hydraulic disconnection would result in oxygen depleted stagnant ponds, leading to GHGs accumulation and evasion. GHG saturations and fluxes were measured in situ using portable gas analyzers. Hydrological isolation was associated with water column stratification, dominance of anoxic bottom water, and elevated CO_2 and CH_4 saturation, approximately 2.6 and 1.6 times higher than when the oxbow lake was connected to the river. River floods and hydraulic connection destratified the water column, restored oxic conditions, and resulted in large nutrient and sediment input to the oxbow lake. Unexpectedly, N_2O saturation remained unchanged across hydrological conditions. This may reflect the combined effects of increased oxygen availability and nitrate supply during river inflow, which can support different N_2O-producing and consuming pathways. These results shed light on multiple mechanisms regulating GHG dynamics during alternating phases of flooding and hydraulic connection, and low discharge and isolation of oxbow lakes.

1. Introduction

In the last centuries, large rivers have experienced extensive hydraulic modifications, including channel straightening, dam construction, embankment building, and the installation of navigation structures such as groynes and weirs (Hudson et al., 2008; Zhang et al., 2021a; Ahmad et al., 2025). These interventions aimed primarily at improving navigation, flood management, hydropower production, and land drainage to expand agriculture (Lang et al., 2003). The main ecological impact of these interventions on the riverine ecosystems is a reduced or lost hydrological connectivity between the main river and the lateral areas, such as floodplains, wetlands, meanders, and oxbow lakes (Knox et al., 2022). The direct consequence of these modifications is the alteration of the functioning of the lateral areas by increasing the aquatic and riparian habitat fragmentation, reducing biodiversity, and increasing erosion and water runoff (Eschbach et al., 2018; Leibowitz et al., 2018). In recent years there has been a growing need for restoration projects under the EU Water Framework Directive and Biodiversity Strategy, aiming at re-establishing complex and variable connectivity between rivers and lateral areas to increase habitat heterogeneity and biodiversity, improve nutrient retention and removal, and reduce greenhouse gas (GHG) emissions (Reckendorfer et al., 2013; Newcomer Johnson et al., 2016; Natho et al., 2020; Maaß et al., 2021).

In recent years GHG emissions have become, on a global scale, one of the key environmental issues. Inland waters are active components of the global carbon (C) and nitrogen (N) cycles, even if they cover only a small surface of our planet (Tian et al., 2016). These ecosystems transport and transform terrestrially derived organic and inorganic C (Cole et al., 2007; Lauerwald et al., 2023), capture carbon dioxide (CO_2) through aquatic primary production, emit CO_2 via heterotrophic mineralization, degassing, and diffusion, bury C in their sediments (Xiao et al., 2024) and have the potential to release large amounts of methane (CH_4) produced in anaerobic sediments (Kirschke et al., 2013). CO_2 and CH_4, together with nitrous oxide (N_2O), are the main GHGs emitted by

* Corresponding author.
E-mail addresses: sara.benelli@unipr.it (S. Benelli), biancamaria.lecchini@unipr.it (B.M. Lecchini), marco.bartoli@unipr.it (M. Bartoli).

https://doi.org/10.1016/j.ecoleng.2026.108145
Received 21 May 2026; Received in revised form 5 August 2026; Accepted 14 August 2026
Available online 20 August 2026

aquatic ecosystems. Emissions of N_2O from inland waters remain poorly investigated, as these ecosystems are generally considered minor sources of this potent GHG (Davidson and Kanter, 2014; Quick et al., 2019). However, in agro-ecosystems inland waters receive significant N inputs due to the leaching of N from manure and synthetic fertilizers (Kumar et al., 2020), resulting in diffuse nitrate (NO_3^-) pollution of surface and groundwater and N_2O production (Seitzinger et al., 2000; Laini et al., 2011).

Wetland restoration interventions may produce contradictory effects on GHG emissions. The reconnection of a lateral area to a river restores oxic and oxidized conditions through water mixing and influx of oxygenated water, suppressing methanogenesis and anaerobic CO_2 production. However, the same reconnection event delivers terrestrial organic matter (OM), promoting aerobic pathways that enhance decomposition of organic C and, ultimately, CO_2 emissions (Borges et al., 2019). Furthermore, river water input enriched with agricultural N runoff can sustain denitrification and N_2O production at redox interfaces (Lauerwald et al., 2023). Nitrous oxide may accumulate as a by-product in the nitrification process and/or as an intermediate in the denitrification process (Quick et al., 2019). In an agricultural context, such as the Po River plain, N_2O may be mainly produced by denitrification of nitrate-rich waters flooding lateral areas (Kumar et al., 2020).

Prolonged periods of lateral hydrological disconnection produce isolated pool habitats, leading to the progressive development of chemically reduced conditions, characterized by depletion of oxygen (O_2), NO_3^-, and sulfate with concurrent accumulation of ammonium (NH_4^+) and of labile OM, favoring methanogenesis and CH_4 accumulation (Borges et al., 2019; Quick et al., 2019). Aside from river discharge, there are other environmental factors that drive GHG emissions in areas temporarily connected to the river, such as water temperature, pH, nutrient concentrations, O_2 and organic matter availability (Wang et al., 2021; Ho et al., 2026). Microbial activity, O_2 consumption, anaerobic to aerobic respiration ratio, and CH_4 and N_2O production increase at high temperature and OM concentrations (Lauerwald et al., 2023). However, the temperature-dependent response is often modulated by multiple riverine ecosystem interactions, including gas solubility, shifts in microbial community composition, reaction kinetics of release, and transport processes (DelSontro et al., 2016). The availability of OM regulates the production of GHGs by acting as the primary electron donor to microbial communities, producing CO_2 through aerobic respiration and CH_4 through anaerobic fermentation (Cole et al., 2007).

Oxygen, the first electron acceptor used by bacteria to mineralize OM, has a strongly negative correlation with CH_4 emissions and a variable relationship with CO_2, depending on the dominant respiratory pathways (Malyan et al., 2022). Suboxic conditions can favor N_2O production because the enzymes catalyzing its reduction to N_2 are inhibited, while nitrite reductase producing N_2O remains active (Zhang et al., 2021b). Generally, freshwater bodies have a pH ranging from 6 to 8, where dissolved inorganic carbon (DIC) is mainly present as bicarbonate. When water becomes more acidic (5), the speciation of the carbonate system shifts from bicarbonate toward dissolved CO_2, increasing the potential for CO_2 evasion to the atmosphere (Malyan et al., 2022). N_2O can be emitted both when the pH has low (< 7) and high (7–8) values, due to two different processes, nitrification and denitrification, respectively (Khoiyangbam and Chingangbam, 2022). Dissolved inorganic N forms further affect GHG emissions (Bodelier, 2011). N can act directly on the methanogenic community. Ammonium can either enhance CH_4 production by relieving N limitation or inhibit methanogenesis when concentrations become high enough to exert toxic or osmotic stress on methanogenic communities (Kim et al., 2015). Nitrate plays a dual role: it can inhibit methanogenesis because it acts as an electron acceptor for alternative respiration pathways that are more energy-efficient than methanogenesis, but at the same time, it is a direct substrate for denitrification, which produces N_2O as a by-product (Kasak et al., 2022).

River-floodplain reconnection has been widely studied in relation to biodiversity, habitat availability, nutrient retention, water quality, and organic-matter processing (Welti et al., 2012; Reckendorfer et al., 2013; Holubová et al., 2016; Newcomer Johnson et al., 2016; Pander et al., 2018). In contrast, less attention has been given to GHG emissions. The limited available evidence has mainly focused on restored riparian wetlands, floodplain soils, or parafluvial sediments rather than on aquatic lateral waterbodies directly reconnected to the main river (Vidon et al., 2014; dos Santos Pinto et al., 2020). This study investigated how alternating periods of hydrological connection and disconnection affect GHG dynamics in the Gussola oxbow lake, a restored lateral waterbody of the Po River in northern Italy. The restoration intervention consisted of the lowering of a navigation groyne, thereby allowing river water to enter the oxbow lake when the Po River discharge exceeds 1500 $m^3 s^{-1}$. This restoration action has substantially increased the frequency of river-oxbow interactions as compared to the pre-intervention period, during which floods occurred with discharge exceeding 4000 $m^3 s^{-1}$ and the oxbow lake consisted of isolated and stagnant ponds. The intervention aims to help reduce further incision processes by dividing the transport capacity between the main course and the oxbow lake. Restoring hydraulic and morphological natural processes is consistent with the Water Framework Directive (2000/60/EC) because lowering the navigation groyne partially restores lateral connectivity between the river and the oxbow lake, increasing inundation frequency and improving hydromorphological functioning. It also supports the Flood Directive (2007/60/EC) by providing additional space for temporary floodwater storage and flow redistribution during high-discharge events. Finally, by restoring the hydrological and morphological processes sustaining floodplain habitats and species, the intervention contributes to the objectives of the Habitats Directive (92/43/EEC). The Gussola intervention exemplifies pilot-phase restoration along the Po River, with some 35 further similar interventions planned for implementation across the basin.

Over one year, we conducted biweekly measurements of GHG saturations and fluxes together with hydrological and physical-chemical variables during river connection, progressive disconnection, isolated-pool conditions. We hypothesized that (i) hydrological isolation of the Gussola oxbow lake from the Po River would trigger anoxic water column conditions and elevated evasion of CH_4 and N_2O; (ii) river water input would restore oxic water column and increase aerobic conditions, reducing the emissions of all GHGs to the atmosphere; and (iii) Po River water inflow would deliver elevated NO_3^- from the agricultural catchment, increasing substrate availability for denitrification and potentially enhancing N_2O production.

2. Materials and methods

2.1. Description of study area and restoration process

The study area is an oxbow lake of the Po River located in the municipality of Gussola (province of Cremona, northern Italy) (Fig. 1). It is a relict meander of the Po River separated from the main channel by an anthropogenic navigation groyne constructed to maintain water depth and gradient for barge traffic. This structure prevented hydraulic connectivity unless the river discharge exceeded 4000 $m^3 s^{-1}$, a high, unusual discharge considering the average value for the Po River is 1500 $m^3 s^{-1}$. In March 2023, the navigation groyne was lowered by 3 m to allow a flow rate exceeding 1500 $m^3 s^{-1}$ to overpass the structure and flood the oxbow lake (Fig. 2).

2.2. GHG saturation and flux measurements

GHG measurements were carried out biweekly from June 2024 to September 2025 at six sampling points across the study area (Fig. 1). Five sites (L1-L5) were located within the oxbow lake, from upstream (L1) to downstream (L5) of the navigation groyne; while one reference station was in the Po River.

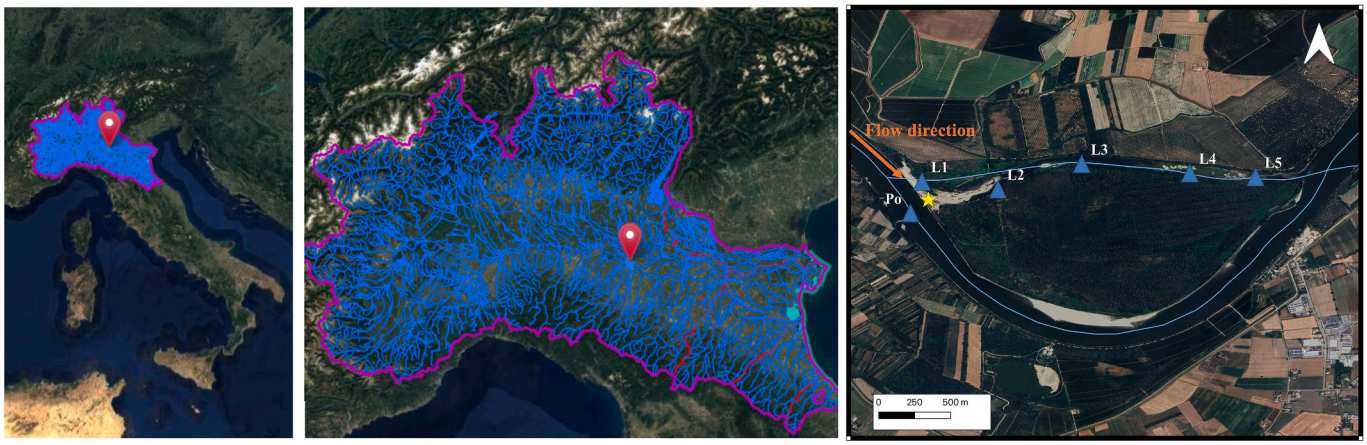

Fig. 1. Location of the study area and sampling points: five stations were distributed across the oxbow lake, and the reference station was the Po River. The yellow symbol indicates the location of the navigation groyne. (For interpretation of the references to colour in this figure legend, the reader is referred to the web version of this article.)

Fig. 2. Oxbow lake during the lowering of the navigation groyne in 2023 (A); oxbow lake two years after intervention during an isolated condition (B); oxbow lake during connection with the Po River (C); the Po River inundating the oxbow lake during an exceptional flood in April 2025 (D).

2.2.1. Saturation measurement

Dissolved CO_2, CH_4, and N_2O concentrations were determined using a bottle headspace equilibration technique adapted from McAuliffe (1971) and Laini et al. (2011). A known volume of in situ water (600 mL) was transferred into a gas-tight bottle fitted with a modified cap and connected to portable gas analyzers (LI-7810 and LI-7820, LI-COR, Lincoln, NE, USA). The bottle was vigorously shaken for 30 s to reach gas equilibrium between the gaseous and the aqueous phases. The analyzers continuously measured the dry mole fractions of CO_2, CH_4, and N_2O in the equilibrated headspace, reported as ppm for CO_2 and ppb for CH_4 and N_2O. Background gas mole fractions in the empty bottle were also measured before headspace equilibration. The total gas volume, including the bottle headspace, connecting tubes, and the internal volume of the analyzers, was determined during instruments calibration by injecting known amounts of CO_2, CH_4, or N_2O into the closed analytical loop.

Gas mole fractions were converted to partial pressures in the equilibrated headspace by multiplying the measured mole fraction by the total gas pressure. The corresponding dissolved concentrations at equilibrium were calculated using Henry's law constants corrected for water temperature. Dissolved gas concentrations in the original water samples were then calculated by correcting gas redistribution between the aqueous phase and the headspace during equilibration (Weiss, 1974; Weiss and Price, 1980). This correction accounted for the difference between the amount of gas in the equilibrated headspace and the amount initially present in the gas phase, considering the total gas volume of the analytical system (headspace, tubing, and analyzer internal volume), gas temperature, total pressure, and sampled water volume. Gas saturation was calculated as the ratio between the calculated dissolved concentration in the water sample and the theoretical concentration expected at equilibrium with ambient air at the measured water temperature.

2.2.2. Flux measurement

A transparent, custom-made floating chamber with a volume of 3.6 L and a surface area of 0.043 m^2, equipped with an internal fan to ensure air mixing, was used to measure gas fluxes at the water-atmosphere interface. The floating chamber was gently positioned on the water surface, with gas tubing connecting the chamber headspace to CO_2/CH_4 and N_2O gas analyzers. Incubations lasted 1 to 3 min to avoid significant changes in air temperature and gas concentration in the headspace. GHG fluxes were derived from floating-chamber deployments by fitting a linear regression to the time series of gas concentration measured in the chamber headspace. The resulting rate of concentration change (ppm s^{-1}) was converted to an areal flux using the chamber headspace volume and surface area, the universal gas constant, and the in situ temperature, with unit conversions applied to express fluxes per hour and in molar units (Ollivier et al., 2019). The volume of the connected tubing, including internal analyzer loops, was included in the effective headspace volume. All measurements were conducted between 9 am and 5 pm local time and from a boat ensuring free movements of the floating chamber with the water current. In this study, we considered only diffusive fluxes, and flux calculations were restricted to incubations with a coefficient of determination (R) of 0.9 or higher.

2.2.3. GHG saturation and flux: rationale of cross-systems and within system comparison

Gas saturations and fluxes were always measured at all sampling stations and were always consistent (Fig. S1). Gas saturation derived from headspace equilibration was used for between-ecosystem comparisons: main river channel, connected and isolated oxbow lake. The rationale of this choice is that the Po River data represent a sort of control, reference condition, whereas the real focus of the study is the comparison of GHG saturations, proxies of fluxes, under connected or isolated hydraulic settings. Gas fluxes measured via floating chambers were assumed to be the same in the Po River and in the oxbow lake during periods of hydraulic connection due to expected similar saturation and water velocity. Gas fluxes were used for within-system spatial comparisons to reveal zonation in the oxbow lake, reflecting environmental gradients (e.g., sediment OM content, oxygen or nutrient concentrations) across the five sampling stations. Floating chambers employed in the oxbow lake were drifting-type (not anchored) to avoid artificial turbulence generation (Lorke et al., 2015).

2.2.4. Global warming potential calculation

Mean CO_2-equivalent fluxes (mg CO_2-eq m^{-2} h^{-1}) were calculated by converting gas fluxes from molar to mass units using their respective molar masses (44, 16, and 44 g mol^{-1}). Fluxes were then multiplied by their 100-year global warming potentials (GWP_{100}) relative to CO_2 (CO_2 = 1, CH_4 = 27, N_2O = 273) according to Forster et al. (2021). The resulting CO_2-equivalent fluxes were obtained by summing the GWP-weighted contributions of each gas. Positive values indicate a net greenhouse gas source to the atmosphere, whereas negative values indicate net uptake.

2.3. Measurement of environmental parameters

At each station and on each sampling date, water samples were collected at a depth of approximately 0.5 m for laboratory analyses. Dissolved inorganic carbon was measured via total alkalinity titration (Dickson, 1981). Briefly, the concentration of carbonates and bicarbonates was determined via fixed end-points titration of the sample with diluted hydrochloric acid (0.1 M). The pH was monitored until the bicarbonate equivalence point, around pH 4.5, was reached. A second aliquot was filtered through a glass fiber filter (GF/F, Whatman) and stored in a scintillation vial to determine the concentrations of dissolved inorganic nitrogen forms (NO_3^-, NH_4^+, NO_2^-) via spectrophotometric techniques (APHA (American Public Health Association), 1992). The filter was then placed in a Teflon vial and analyzed by extraction with 90% acetone followed by spectrophotometric measurement of chlorophyll *a* (Lorenzen, 1967). Samples of molecular nitrogen (N_2) were collected via overflushing 12-mL screw-cap vials (Exetainer®, Labco Limited, UK) and adding 100 µL of 7 M $ZnCl_2$ to stop microbial activity. The analysis was carried out using a membrane inlet mass spectrometer (MIMS, Bay Instruments). Calculations were based on N_2/Ar ratio measurements (Kana et al., 1994). Additional parameters were measured in situ with a multiprobe (YSI model 556), recording water temperature, electrical conductivity (EC), pH, oxidation-reduction potential (ORP), and dissolved O_2 concentration. We gathered river discharge data from the ARPAE-SIMC Dext3r data portal (https://simc.arpae.it/dext3r/), with daily mean discharge recorded at the Boretto (province of Reggio Emilia) monitoring station located approximately 10 km downstream of the study site.

2.4. Statistical analysis

All statistical analyses were performed using R Studio software (R Core Team, 2025). Water-chemistry differences among hydrological conditions (Po River, connected and isolated oxbow lake) were analyzed using linear mixed-effects models (LMMs). Mixed models were selected because the dataset consisted of repeated measurements collected from the same stations on multiple sampling dates, resulting in non-independent observations and an unbalanced number of samples among hydrological conditions. For each response variable, hydrological condition (Group, three levels) was treated as a fixed effect as differences among conditions were the primary focus of the analysis. Sampling date and station were included as random intercepts to account for repeated measurements and the unbalanced number of observations across groups (*lme4* package). Overall group effects were assessed with F-tests from the mixed-model ANOVA table (*lmerTest* package). When the Group effect was significant, post-hoc pairwise comparisons among the three groups were performed on model-based estimated marginal means (EMMs) using Tukey-adjusted contrasts (*emmeans* package). To control for multiple testing across the set of response variables, *p*-values for the overall Group effect were additionally adjusted using the Benjamini–Hochberg false discovery rate (FDR) procedure.

GHG saturation and flux data were analyzed on the logarithmic scale to reduce skewness and to ensure Gaussian distribution. For CO_2 and N_2O flux data, which included zero or slightly negative values, a small constant (0.01) was added before transformation. Methane fluxes, which were always positive, were log-transformed directly. To evaluate the effect of hydrological condition on GHG saturation, Gamma generalized linear mixed models (GLMMs) were applied with a log link using the *glmmTMB* package. The fixed effect was the hydrological condition that consisted of a three-level factor (Group): the Po River, the oxbow lake connected to the river, and the oxbow lake when it was isolated from the river. The random intercepts were included for sampling date and station to account for repeated measurements. Because residual variability differed among hydrological condition groups, we applied a group-specific dispersion. Model fit and assumptions were evaluated using simulation-based residual diagnostics with DHARMa, including tests for outliers and overdispersion. Group-level estimates were obtained as EMMs with 95% confidence intervals on the response scale (% saturation), and pairwise comparisons among the three groups were performed using Tukey-adjusted contrasts (*emmeans* package).

To assess whether floating-chamber fluxes and gas saturation measurements provide comparable relative differences among oxbow lake stations, we restricted the analysis to the disconnected period and to the five oxbow lake stations (L1–L5). Since fluxes and saturation are in different units, we standardized responses to z-scores and fitted linear mixed-effects models with method, station, and their interaction as fixed effects and sampling date as a random intercept. A non-significant method × station interaction was interpreted as evidence that both methods capture consistent spatial patterns among stations. For each gas

flux (already log-transformed), LMMs were fitted with station as a fixed effect and sampling date as a random intercept. The effect of station was tested using F-tests from these models (*lme4* and *lmerTest* packages). When the station effect was significant, Tukey-adjusted pairwise comparisons of EMMs were performed.

To evaluate the relationship between GHG emissions and the environmental variables, a multivariate analysis was conducted using the package *vegan* for ordination and permutation tests and *corrplot* for visual exploration of correlations among predictors. Prior to constrained ordinations, collinearity among environmental predictors was evaluated using Pearson correlation matrices. Correlations were visualized with correlation plots. When strong collinearity occurred among groups of variables ($|r| > 0.70$), a subset of predictors was retained for modeling. The variance inflation factor (VIF <2) was also monitored as an indicator to reduce the collinearity among explanatory variables (Zuur et al., 2010). Patterns in the environmental dataset were explored using principal component analysis (PCA) on centered and scaled environmental variables. PCA was used to visualize major environmental gradients and to assess the separation of samples by hydrological condition (connected vs isolated). To relate multivariate GHG patterns to hydrological connectivity and environmental drivers, a redundancy analysis (RDA) was applied using log-transformed GHG saturations as the multivariate response matrix (Oksanen et al., 2022). Environmental predictors were selected using forward selection with permutation tests and an adjusted (R^2) stopping criterion (ordiR2step in *vegan*; 999 permutations). The final model was evaluated with permutation tests to assess its overall significance, the significance of individual axes, and for the marginal contribution of each predictor. Tests were performed using the 'anova()' function in the *vegan* package, with statistical significance set at $p < 0.05$. RDA results were interpreted based on the scaling 2. Angles between all vectors reflect linear correlation (Legendre and Legendre, 1998). A 5% significance threshold was set for all statistical tests. Figures were made using ggplot2 (Wickham, 2006), and correlation matrices were displayed with corrplot (Wei et al., 2017).

3. Results

3.1. Hydrological conditions during the sampling period and water chemistry

From June 2024 to September 2025, the discharge of the Po River fluctuated substantially (Fig. 3). Discharge during June–July 2024 was elevated due to summer precipitation events, reaching 2500–4000 m^3 s^{-1} on several occasions. Throughout most of 2025, the river discharge remained below 1500 m^3 s^{-1} (dashed red line in Fig. 3). A major flood event on April 20th reached nearly 7000 m^3 s^{-1}, representing one of the largest floods in the last century. From June to September 2025, discharge mainly fell below 1500 m^3 s^{-1}. Overall, during the monitoring period, the oxbow lake was hydrologically connected to the Po River for approximately 28% of the total sampling period and remained isolated for 72%. However, prior to the requalification works, hydraulic connectivity between the Po River and the oxbow lake was achieved only under high-flow conditions, corresponding to a discharge threshold of approximately 4000 m^3 s^{-1} (solid red line in Fig. 3). Applying this pre-intervention threshold to the study period, river water would have entered the oxbow lake for only 14 days, compared with 135 days classified as connected under the post-intervention threshold, indicating that the intervention reduced the discharge threshold for the onset of river–oxbow lake connectivity and increased the frequency and duration of lateral exchange.

Water chemistry differed between hydrological conditions (Fig. 4). Based on the overall mixed-effects model tests, the strongest evidence for group differences was observed for NO_3^- concentration ($p = 0.001$), conductivity ($p = 0.001$) and DIC ($p = 0.003$). pH also differed among groups, although with weaker support ($p = 0.039$), and no statistically supported differences were detected for the other parameters. Post-hoc Tukey-adjusted pairwise comparisons indicated that the isolated oxbow lake was the condition that most consistently differed from the other groups (Table S1). During the periods when the oxbow lake was hydrologically connected to the river, no significant differences in water chemistry were observed between the two systems. In contrast, significant variations in several measured parameters were detected between the isolated and connected phases of the oxbow lake. Specifically, DIC and N_2 concentrations, and conductivity were higher during the isolated condition, whereas NO_3^- concentration and pH were significantly lower

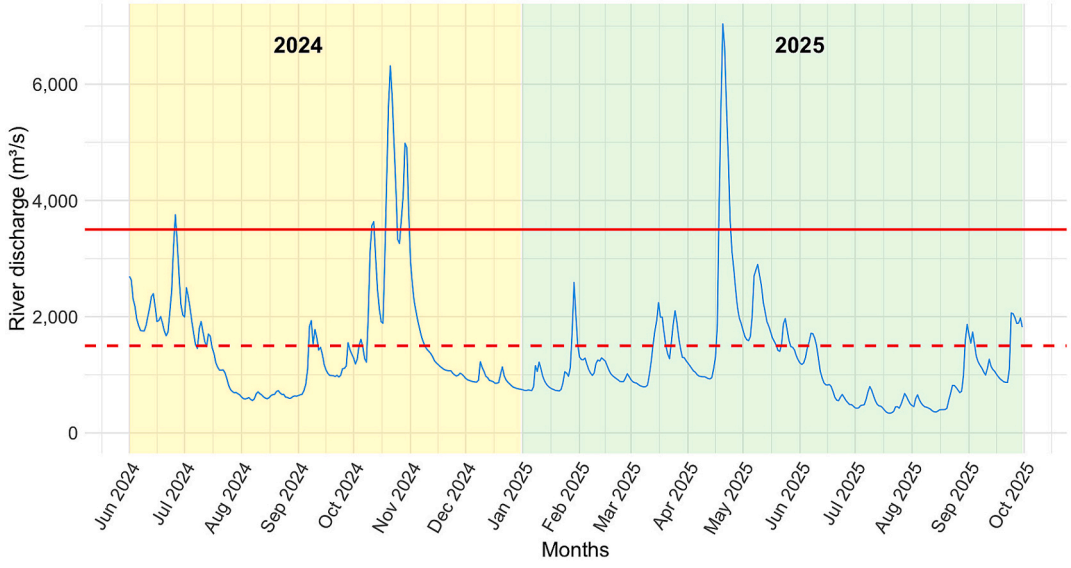

Fig. 3. The Po River discharge recorded during the monitoring period. The dashed red line indicates the post-intervention discharge threshold for Po River inflow into the oxbow lake, whereas the solid red line denotes the pre-intervention threshold (4000 m^3 s^{-1}). (For interpretation of the references to colour in this figure legend, the reader is referred to the web version of this article.)

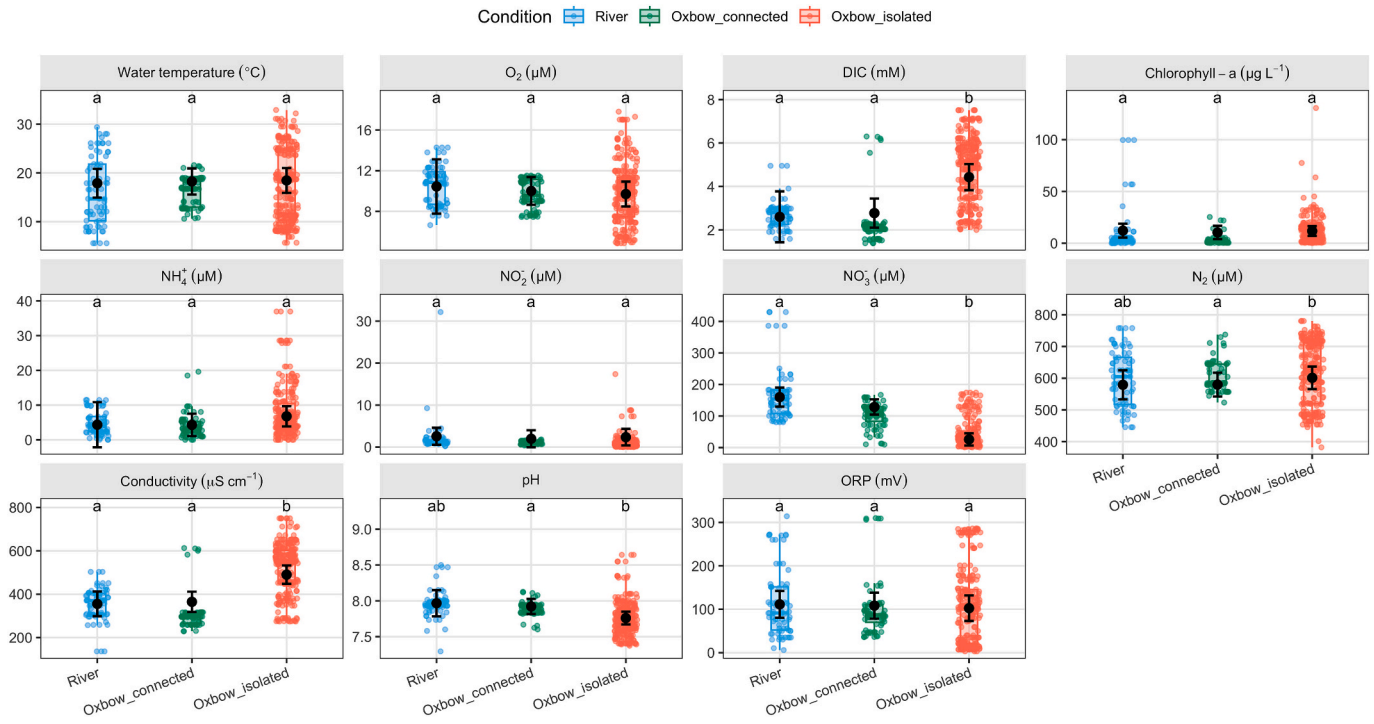

Fig. 4. Water chemistry across hydrological conditions (Po River, oxbow lake connected and isolated). Boxplots and points show individual observations. Black circles and vertical error bars represent model-based estimated marginal means (EMMs) ± 95% confidence intervals from linear mixed-effects models. Different letters above groups indicate significant differences among conditions based on Tukey-adjusted pairwise contrasts.

when water became more stagnant. The water chemistry of the Po River differed from that of the isolated oxbow lake primarily in conductivity, DIC and NO_3^- concentrations.

3.2. GHG saturation between-ecosystem comparisons

GLMMs showed contrasting GHG responses to hydrological conditions (Fig. 5). CO_2 saturation differed significantly among groups ($p < 0.001$). EMMs were similar between the river (318%; 95% CI: 248–408) and the connected oxbow lake (370%; 286–478), and markedly higher during oxbow lake isolation (952%; 754–1200). The calculated coefficient of variation (CV) increased from the river (32%) to the connected (69%) and the isolated oxbow lake (86%). Tukey-adjusted pairwise contrasts showed no difference between the river and the connected oxbow lake ($p = 0.560$), whereas CO_2 saturation in the isolated oxbow lake exceeded both the river ($p < 0.001$) and the connected oxbow lake ($p < 0.001$). Relative to the connection phase, isolation increased CO_2 saturation 3.0- and 2.6-fold compared to the river site and the connected oxbow lake, respectively.

Methane saturation showed a similar pattern (Fig. 5). EMMs CH_4 were 16,127% (10,968–23,714), 21,229% (14,123–31,911), and 34,900% (24,217–50,294) in the river, the connected and the isolated oxbow lake, respectively. The latter showed extremely high dispersion (CV = 171%), consistent with pronounced heterogeneity and episodic high-saturation events relative to the mean. In comparison, CH_4 variability was lower in the Po River (CV = 50%) and intermediate during connected conditions (CV = 73%). Methane saturation measured in the oxbow lake during isolation was significantly higher than the river ($p = 0.001$) and the connected oxbow lake ($p = 0.036$). The level of CH_4 saturation was 1.6- and 2.2-fold higher than in the river and the connected oxbow lake, respectively. In contrast to CO_2 and CH_4, N_2O saturation did not differ significantly among hydrological conditions ($p = 0.697$) (Fig. 5). Saturation values were 172% (160–185) in the river, 172% (159–187) in the connected oxbow lake, and 178% (165–193) in the isolated condition. Indeed, N_2O saturation was less variable among environments: in the Po River and in the connected oxbow lake N_2O variability was around 15%, while variability increased during oxbow isolation (CV = 37%). Tukey-adjusted pairwise contrasts indicated no significant differences (all $p \geq 0.71$).

3.3. Spatial variability of GHG fluxes across the oxbow lake

The comparison between gas saturation and chamber flux measurements yielded similar station rankings and spatial patterns (Fig. S1). When isolated, the oxbow lake showed significant spatial differences among stations for CO_2 ($p < 0.001$) and CH_4 ($p = 0.039$), but not for N_2O ($p = 0.320$). For CO_2 fluxes, the station effect was strong, with the upstream stations (L1 and L2), located close to the navigation groyne and to the riverine input, exhibiting the highest fluxes. Fluxes at L1 and L2 stations were significantly higher than fluxes at L5, while fluxes at L2 also exceeded fluxes at L4 (Fig. 6). On the original flux scale, these differences corresponded to approximately a 2-fold higher CO_2 efflux at upstream stations (L1−L2) than at the most downstream sites (L4–L5), revealing a clear longitudinal gradient in CO_2 emissions along the oxbow lake when it is isolated.

Differences among stations were also significant for CH_4 fluxes. Station L2 exhibited approximately 3-fold higher CH_4 fluxes on the original scale compared to station L4 (Tukey contrast $p = 0.041$), consistent with a water residence time gradient that favors CH_4 accumulation at upstream locations. Spatial analysis within the isolated oxbow revealed no significant differences in N_2O fluxes among the five stations ($p = 0.320$), indicating spatially uniform N_2O concentrations that appear decoupled from the biogeochemical gradients controlling CO_2 and CH_4.

3.4. Significant environmental drivers of GHG emissions from the oxbow lake

The RDA revealed significant differences in log-transformed GHG saturations between connected and isolated hydrological conditions (p

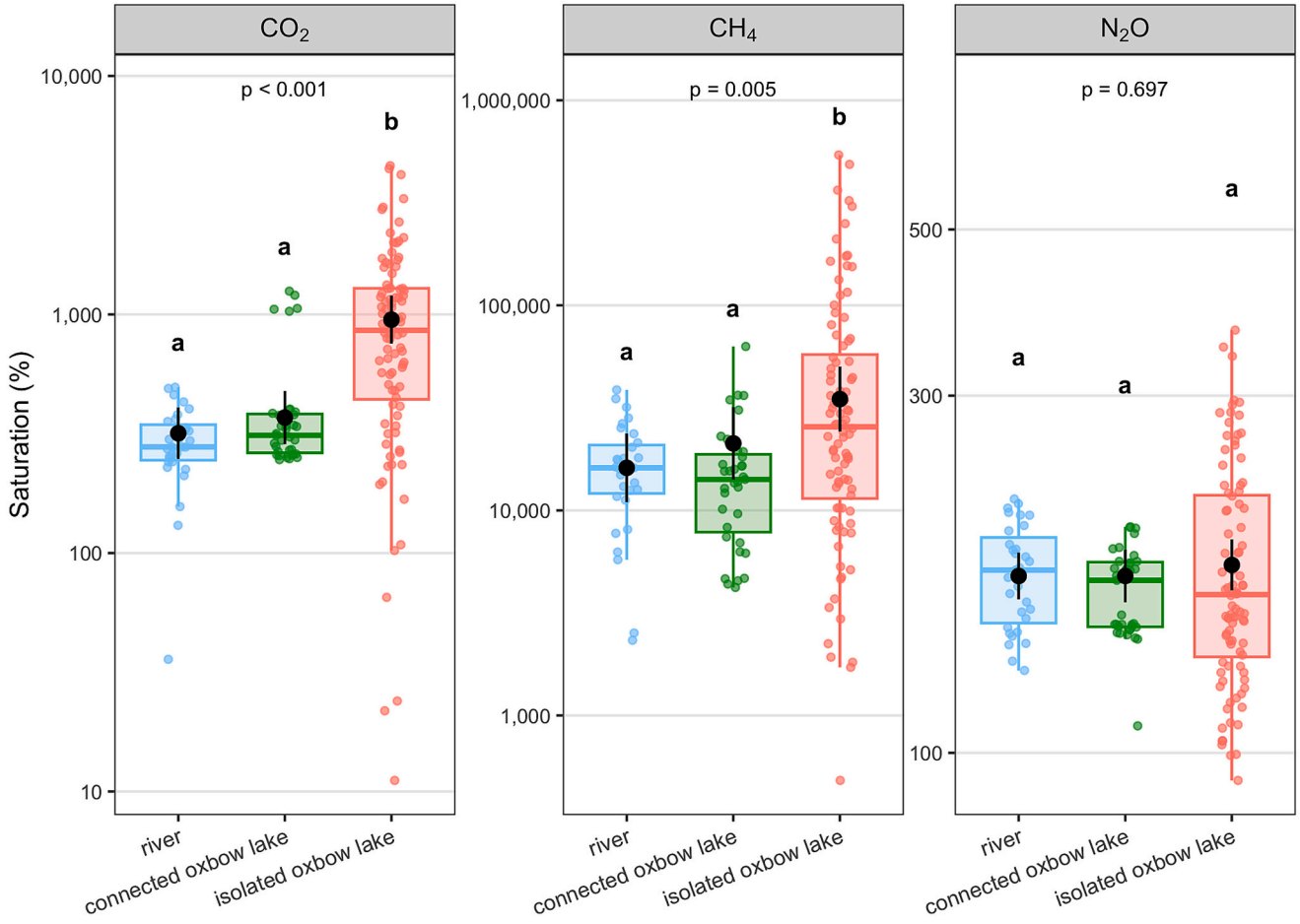

Fig. 5. Saturation of greenhouse gases across hydrological conditions (Group). Boxplots show gas saturation (%) for CO_2, CH_4, and N_2O in the Po River, and in the oxbow lake during connected and isolated conditions (points = individual Date*Station observations). Black circles and vertical error bars represent model-based EMMs ±95% confidence intervals from Gamma GLMMs. Different letters indicate significant differences between conditions based on Tukey-adjusted pairwise contrasts ($p < 0.05$). The y-axis is plotted on a $\log_{10}$ scale to account for magnitude differences while keeping percent saturation units constant.

= 0.001). The final RDA model, which included hydrological condition (Connection) and selected environmental predictors (DIC, N_{2w}, O_2, pH, NH_4^+), explained 67.4% of the total variance in the GHG response (R^2 = 0.674; R^2 adj = 0.668). The first axis (RDA1) accounted for 56.6% of the total variance, while the second axis (RDA2) contributed an additional 10.2%. RDA3 contributed <1% of the total variance and it was not interpreted. The hydrological condition remained a significant factor in the final RDA model ($p = 0.008$), explaining part of the variability in GHG saturation independently of the environmental predictors. Marginal term tests showed significant contributions for all retained predictors ($p \leq 0.011$) (Table S2).

Measurements from isolated oxbow lake sites reported in Fig. 7 were more dispersed along the RDA1 axis, whereas samples collected during the connection of the oxbow lake to the river showed more clustering along the RDA2 axis. RDA1 was primarily associated with DIC and NH_4^+ concentrations, which are positively related to logCO_2 and logCH_4. RDA2, although significant, explained a smaller proportion of the variance and was related to variations in O_2 and pH (positive scores) and N_{2W} (negative score). LogN_2O was closer to the origin and slightly shifted toward the high-pH, high-O_2 area of the gradient.

When comparing GHG saturations during the isolated phase of the oxbow lake, the final model was highly significant ($p = 0.001$) and explained 68.2% of the total variance in the GHG response ($R^2 = 0.681$; R^2 adj = 0.669). RDA1 accounted for 54.5%, RDA2 for 12.7%, and RDA3 only for 1% of the total variance. Station identity remained significant in marginal test, indicating differences among stations beyond the measured environmental covariates (Table S3). Among the environmental predictors, N_{2w} and DIC accounted for the largest unique fractions of explained variance, followed by pH and dissolved O_2; ORP had a smaller but significant effect. The distribution of stations in the RDA plot revealed that L1 and L2 stations were more closely associated with higher concentrations of logCO_2 and logCH_4, while L3, L4, and L5 stations showed greater variation along the RDA2 (Fig. 8).

4. Discussion

4.1. Effects of hydrological connectivity on CO_2 and CH_4 dynamics

River inflow significantly reduced CO_2 and CH_4 saturation levels and fluxes in the oxbow lake; however, both gases remained consistently supersaturated. Similar results are reported by Lew et al. (2025) that analyzed CH_4 and CO_2 fluxes along a lotic-lentic hydrological gradient, revealing significantly higher emissions in disconnected versus connected floodplain lakes. During connected periods, the anaerobic respiration pathways are replaced by aerobic processes due to the influx of NO_3-enriched water. Indeed, monitoring actions targeting water chemistry demonstrate shortly after the disconnection of the oxbow lake from the Po River a rapid consumption of NO_3^- and O_2 and the establishment of hypoxic conditions in the subsurface water layers (data not shown). There are multiple possible explanations for decreased CO_2 and CH_4 saturation levels during hydraulic connection. Under oxic conditions, the redox potential and the availability of electron acceptors to

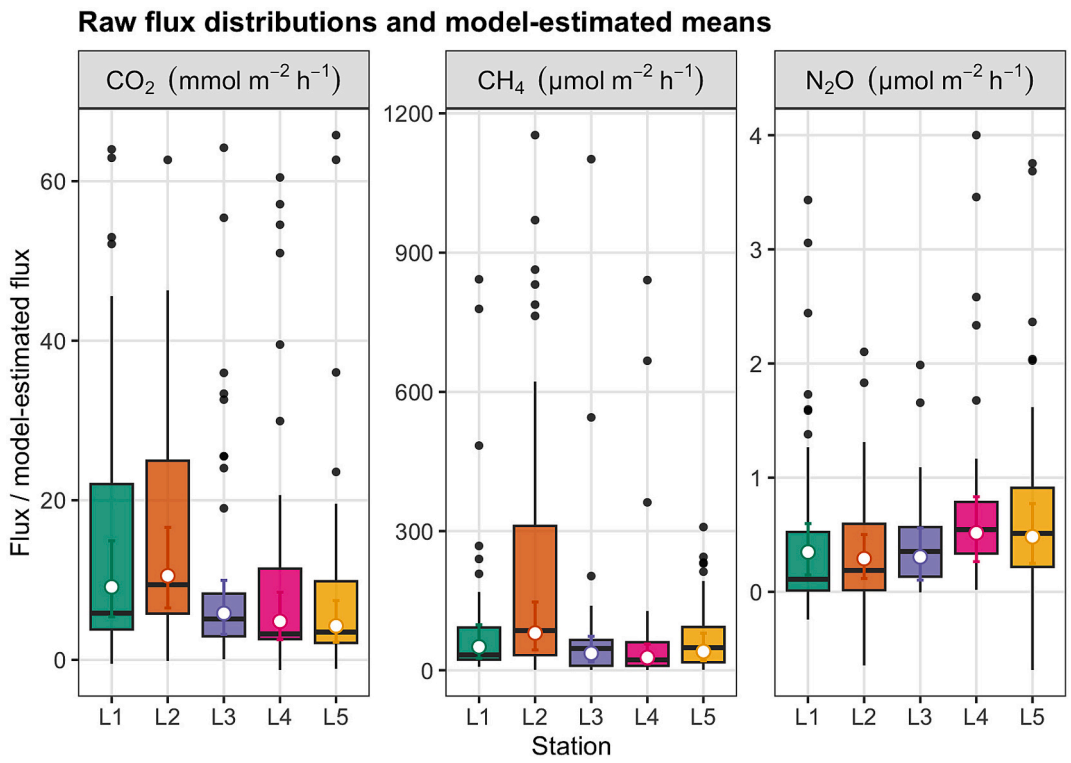

Fig. 6. Boxplots show the distribution of GHG fluxes at each station. Solid horizontal lines show medians; boxes are the interquartile range, and whiskers are the minimum-maximum values. Black dots denote outliers. White circles indicate model-estimated mean fluxes (± 95% CI) from linear mixed-effects models (log-transformed fluxes with sampling date as a random intercept), back-transformed to the original units (CO_2 in mmol m^{-2} h^{-1}; CH_4 and N_2O in µmol m^{-2} h^{-1}).

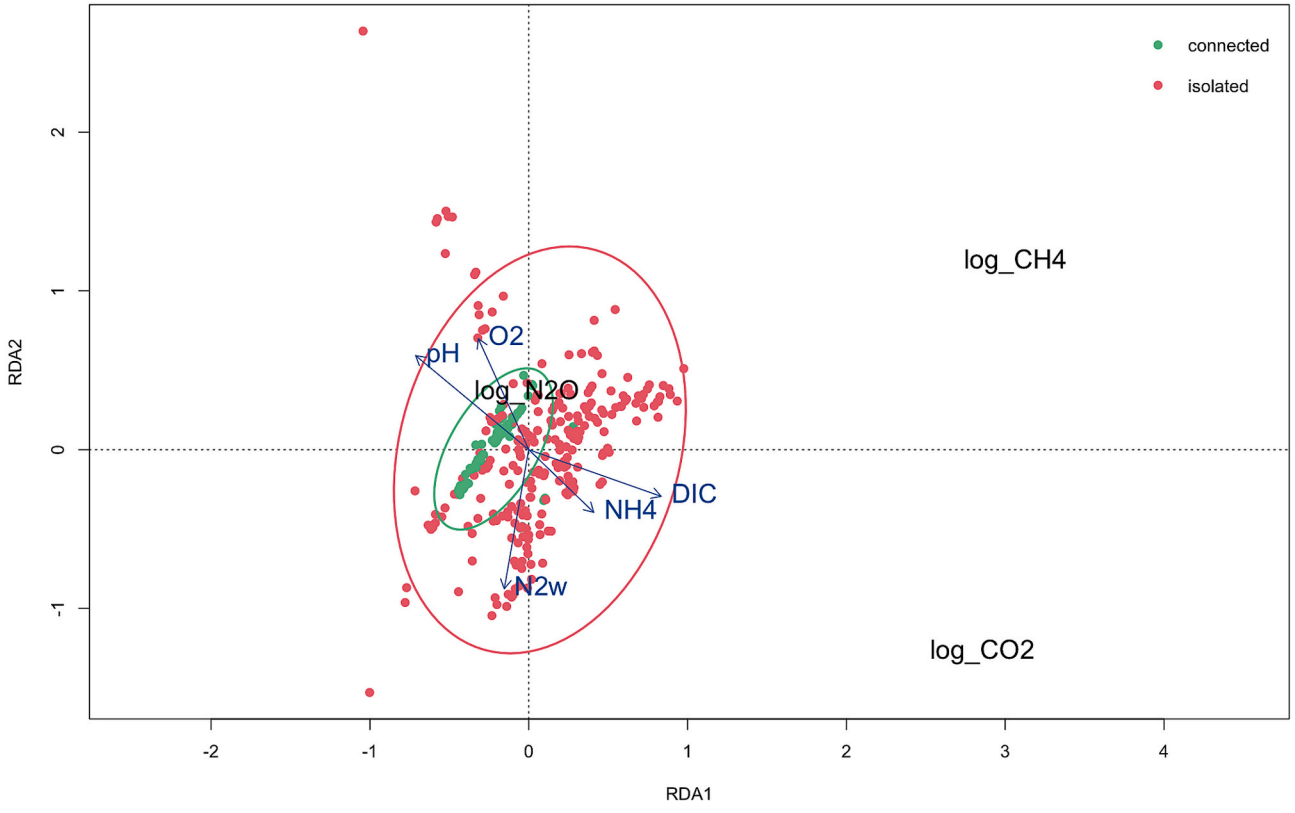

Fig. 7. Redundancy analysis triplot (scaling 2) showing the joint variation of log-transformed CO_2, CH_4, and N_2O saturation in the oxbow lake related to key environmental gradients. Vectors indicate the direction of increasing gas saturations (black labels) and environmental variables (blue labels). Symbols represent station–date combinations, colored by hydrological condition. (For interpretation of the references to colour in this figure legend, the reader is referred to the web version of this article.)

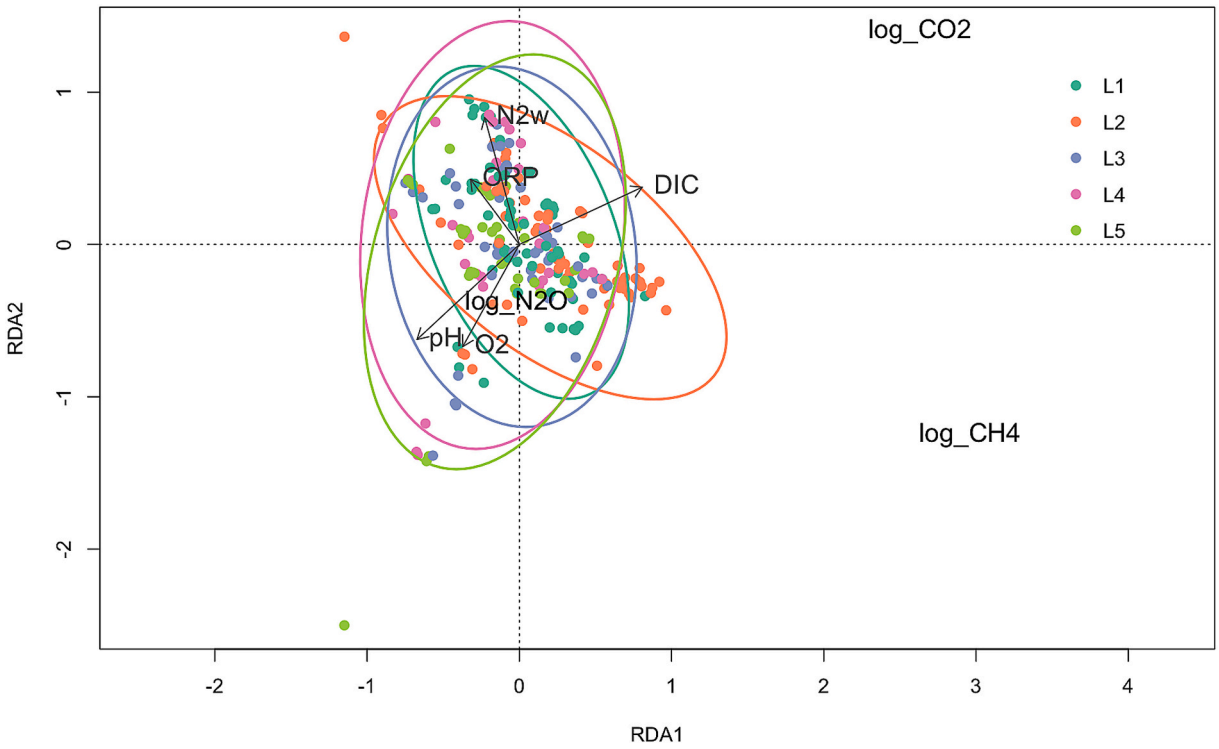

Fig. 8. Redundancy analysis triplot (scaling 2) showing the joint variation of log-transformed CO_2, CH_4, and N_2O saturation among the five stations sampled within the oxbow lake related to key environmental gradients. Vectors indicate the direction of increasing gas saturations (black labels) and environmental variables (grey labels). Symbols represent replicate–date combinations, colored by station.

degrade the OM increase. The presence of O_2 suppresses methanogenic enzyme activity in both the water column and sediment, and simultaneously oxic conditions promote aerobic methanotrophy at the oxic-anoxic interface, where aerobic methanotrophs oxidize CH_4 to CO_2 (Cui et al., 2024; Lew et al., 2025). Water mixing and flow rate reduce residence time, limiting the accumulation of reduced metabolites (DIC, NH_4^+) and of the autochthonous OM that fuels the heterotrophic respiration. Additionally, the dynamic mixing action of flowing water reduces water column stratification, a condition that in isolated oxbow lakes maintains steep O_2 gradients and confines anoxic mineralization to bottom waters where accumulated CO_2 cannot readily escape.

Hydrological isolation of the oxbow lake from the Po River creates conditions that progressively promote autotrophy in surface water and anoxic heterotrophy in bottom waters: nutrients derived from internal sources are no longer diluted or exported downstream, resulting in nutrient enrichment and enhanced primary production, as commonly observed in hydrologically isolated floodplain backwaters and lakes (Zeng et al., 2025). Indeed, increased water residence time and nutrient retention in disconnected water bodies stimulate phytoplankton growth and enhance autochthonous organic matter production, with phytoplankton-derived carbon often dominating the particulate organic matter pool (Reckendorfer et al., 2013). If blooming phytoplankton has the potential to decrease CO_2 saturation, such a decrease is contrasted by heterotrophic respiration in OM rich sediments, receiving post bloom labile algal biomass (Xiao et al., 2020). Our data suggest that during isolation periods photosynthesis by phytoplankton decreases CO_2 oversaturation, but not to an extent that reverse effluxes. Oxygen profiles, not shown in this work, suggest that photosynthesis is constrained by limited light penetration and that the shallow water column is stratified during isolation periods. Benthic respiration consumes O_2 progressively, shifting the system toward hypoxia and ultimately anoxia (Müller et al., 2012). Under anoxic conditions, OM mineralization shifts toward anaerobic metabolic pathways following the sequential depletion of energetically favorable electron acceptors, ultimately leading to methanogenesis in freshwater sediments (Burgin and Hamilton, 2007). Our data align with these mechanisms, as CH_4 saturation is significantly higher in isolated versus connected periods.

A strong longitudinal gradient in CO_2 emissions was found along the isolated oxbow lake (2-fold higher at upstream stations L1-L2 vs downstream L4-L5), which reflects variation in water residence time and organic matter mineralization. Indeed, upstream reaches immediately downstream of the navigation groyne experience earlier stagnation and maintain stronger stratification for longer periods, accumulating OM and DIC before water gradually moves downgradient (Holubová et al., 2016). We believe that under disconnected conditions the turbidity of the eutrophic Gussola oxbow lake limits phytoplankton production to a thin surface water layer and that heterotrophic benthic and pelagic respiration and OM mineralization are significant sources of CO_2, consistent with observations from similar freshwater systems (Waldron et al., 2007).

4.2. *Effects of hydrological connectivity on N_2O dynamics*

N_2O always displayed a low oversaturation suggesting that its production was moderate as compared to diffusive emissions. This intermediate of both nitrification and denitrification was consistently oversaturated in both the Po River and in the oxbow lake. However, its dynamics contrasted sharply with those of CO_2 and CH_4, showing no detectable response to changes in hydrological connectivity and only weak spatial structure within the oxbow lake. An alternative explanation for similar saturation values under different conditions (i.e., connected oxic vs. isolated suboxic) is a shift in the dominant N_2O-producing process (e.g., from nitrification to denitrification), resulting in similar saturation values. Across hydrological conditions, N_2O saturation remained narrowly constrained around 170–180%, with overlapping confidence intervals between the river, the connected oxbow lake, and the isolated phase, and coefficients of variation that were 2–3 times lower than for CO_2 and CH_4. This moderate but persistent

supersaturation aligns with previous findings in rivers, lakes, and small reservoirs, where N_2O usually shows a smaller dynamic range than CH_4 and only shows limited lateral variability despite strong gradients in C metabolism and hydrology (Borges et al., 2019). In our system, the absence of a connectivity effect on N_2O contrasts with patterns reported for some floodplains and restored wetlands in agricultural landscapes, where the enhanced hydrological exchange increases NO_3^- retention and removal via complete denitrification (Hanrahan et al., 2018). For instance, Welti et al. (2012) showed that when riverine water was added to a disconnected floodplain site, mimicking a reconnection event, the N_2O:N_2 ratio decreased, increasing the fraction of denitrification ending as N_2, whereas the opposite pattern emerged when backwater-derived water was added to a restored site, simulating a prolonged disconnection and resulting in higher N_2O relative to N_2 production. In a previous study carried out in the same geographical area, Ribaudo et al. (2023) reported significantly higher diffusive N_2O fluxes in nitrate-rich connected wetlands (67 to 1029 nmol m^{-2} h^{-1}) than in nitrate-poor isolated wetlands (−15 to 173 nmol m^{-2} h^{-1}). Our measured fluxes (619 ± 413 and 573 ± 674 nmol m^{-2} h^{-1} under connected and isolated conditions, respectively) indicate that neither the transition from connected to isolated conditions nor the along-oxbow lake gradients in residence time and sediment-driven C processing produced measurable changes in N_2O saturation. This is consistent with experimental evidence showing that increasing hydrological connection of the floodplain can enhance NO_3^- retention and favor more complete denitrification without necessarily amplifying N_2O emissions (Welti et al., 2012; Hanrahan et al., 2018). The RDA places logN_2O close to the multivariate origin, with only a slight association with higher pH and O_2 concentration and not clearly separated conditions (i.e., connected versus isolated).

4.3. *Increased hydrological connectivity: implications for restoration design and climate mitigation*

The lowering of the navigation groyne increased the hydrological connectivity between the Po River and the Gussola oxbow lake by a factor of nearly 10, from approximately 14 days (under pre-intervention conditions, with connection at >4000 m^3 s^{-1}) to 135 days (under post-intervention conditions, with connection at >1500 m^3 s^{-1}). This significantly longer period of hydraulic connection is important and justifies the present and other analogous studies. Indeed, during connectivity events, the influx of river water at elevated discharge alters the physical structure of the oxbow lake: depths fluctuate, substrate composition shifts, and the original bathymetry is progressively modified. During flood pulses, the river delivers allochthonous OM in the form of suspended particulate organic carbon, dissolved organic carbon, and macroscopic plant detritus that settles within the oxbow lake when the flow velocity is reduced (dos Santos Pinto et al., 2020). Such OM input has the potential to change the biogeochemical processes occurring in the oxbow lake by enriching the sediment pool with labile substrates and increasing microbial heterotrophic activity (Hudson et al., 2008). Furthermore, flood pulses mobilize previously buried OM, mixing old and recent particles, affecting the redox matrix within sediments and increasing mineralization and nutrient cycling, as reported in sediments with bioturbating macrofauna (Aller and Cochran, 2019). Groyne lowering at the study site aimed at reducing riverbed incision and modulating solid transport. It also provided a valuable opportunity to examine how more frequent connection affects GHG saturations and fluxes at the Gussola oxbow lake, which is the focus of the present study. Other environmental aspects, including microbially-mediated biogeochemical cycles, macrophytes, fish and birds communities, are also monitored within much longer investigation programs. Similar successful river restoration actions were carried out in other large European rivers such as the Danube River. Holubová et al. (2016) demonstrated that by lowering navigation groynes, multiple benefits are provided, including increased habitat diversity in the main channel, reduced riverbed incision, and higher sustainability of the restored hydrological connectivity while the navigation conditions can be maintained.

The differential response of CO_2 and CH_4 compared to N_2O has important implications for restoration strategies along the Po River. In our study, the total GHG flux, expressed in CO_2-equivalents, was 553 and 203 mg CO_2-eq m^{-2} h^{-1} when the Gussola oxbow lake was isolated and connected, respectively, suggesting a 63% reduction following the restoration action. Regardless the hydrological condition the total GHG flux was strongly dominated by CO_2 (Fig. 9). In the connected oxbow lake, CO_2, CH_4 and N_2O accounted for 86.2, 10.1, and 3.7% of the total warming potential, respectively, whereas in the isolated oxbow lake their contributions were 90.3, 8.3, and 1.3%. A similar share of the three gases contribution (87, 9, and 4%) is reported by Koschorreck et al. (2026) in riverine station of the Elbe River. These results indicate that, despite the high global warming potential of N_2O, its contribution to the overall GHG budget remains minor relative to CO_2 and CH_4.

In lowland European rivers with similar geomorphology and agricultural pressures, enhancing hydrological connectivity may therefore yield tangible climate benefits by reducing CO_2 and CH_4 emissions from lateral waterbodies. In our system, the increase in connectivity from 14 to 135 days per year was associated with a substantial reduction in the warming potential driven by these two gases. By contrast, this mitigation signal does not extend to N_2O, whose relative contribution remains low and appears largely insensitive to changes in river–oxbow lake connectivity. Overall, these findings suggest that restoration strategies aimed at increasing hydrological connectivity can effectively reduce the climate impact of fluvial wetlands, primarily through their influence on CO_2 and CH_4 dynamics, while having limited effects on the contribution of N_2O to the total greenhouse gas budget.

Declaration of generative AI and AI-assisted technologies in the manuscript preparation process

During the preparation of this work the authors used chatGPT in order to improve language and the readability of the manuscript. After using this tool, the authors reviewed and edited the content as needed and take full responsibility for the content of the published article.

CRediT authorship contribution statement

Sara Benelli: Writing – review & editing, Writing – original draft, Investigation, Formal analysis, Data curation, Conceptualization. **Bianca Maria Lecchini:** Writing – review & editing, Investigation.

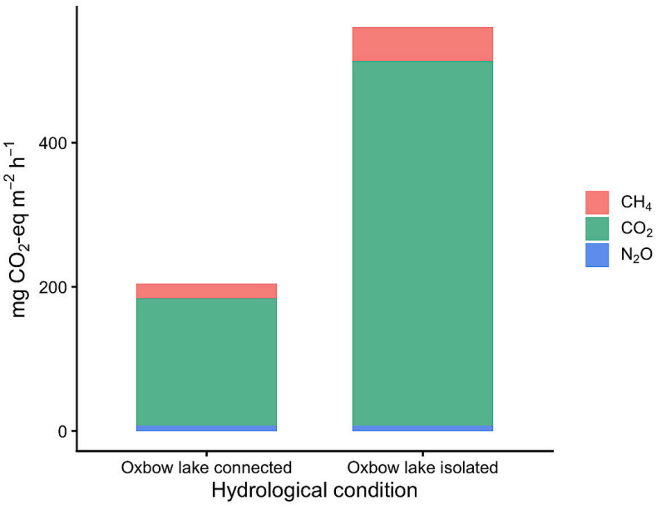

Fig. 9. Mean GHG fluxes expressed as CO_2-equivalents under connected and isolated hydrological conditions. Bars represent the average contributions of CO_2, CH_4, and N_2O to the total greenhouse gas flux, calculated across sampling stations and dates (mg CO_2-eq m^{-2} h^{-1}).

Marco Bartoli: Writing – review & editing, Validation, Supervision, Project administration, Funding acquisition, Conceptualization.

Declaration of competing interest

The authors declare that they have no known competing financial interests or personal relationships that could have appeared to influence the work reported in this paper.

Acknowledgments

This research project was funded by the European Union. The work described in this publication was subsidized by Horizon Europe (HORIZON) framework by the Grant Agreement Number 101056804. Views and opinions expressed are however those of the author(s) only and do not necessarily reflect those of the European Union or CINEA. Neither the European Union nor the granting authority can be held responsible for them.

Appendix A. Supplementary data

Supplementary data to this article can be found online at https://doi.org/10.1016/j.ecoleng.2026.108145.

Data availability

Data will be made available on request.

References

Ahmad, H., Miranda, L.E., Dunn, C.G., Boudreau, M.R., Colvin, M.E., 2025. Hydrologic connectivity in floodplain systems: a multiscale review of concepts, metrics and management. Hydrol. Process. 39 (9), e70260. https://doi.org/10.1002/hyp.70260.

Aller, R.C., Cochran, J.K., 2019. The critical role of bioturbation for particle dynamics, priming potential, and organic C remineralization in marine sediments: local and basin scales. Front. Earth Sci. 7, 157. https://doi.org/10.3389/feart.2019.00157.

APHA (American Public Health Association), 1992. Standard Methods for the Examination of Water and Wastewaters, Washington DC, 18th ed.

Bodelier, P.L.E., 2011. Interactions between nitrogenous fertilizers and methane cycling in wetland and upland soils. Curr. Opin. Environ. Sustain. 3 (5), 379–388. https://doi.org/10.1016/j.cosust.2011.06.002.

Borges, A.V., Darchambeau, F., Lambert, T., et al., 2019. Variations in dissolved greenhouse gases (CO_2, CH_4, N_2O) in the Congo River network overwhelmingly driven by fluvial-wetland connectivity. Biogeosciences 16, 3801–3834. https://doi.org/10.5194/bg-16-3801-2019.

Burgin, A.J., Hamilton, S.K., 2007. Have we overemphasized the role of denitrification in aquatic ecosystems? A review of nitrate removal pathways. Front. Ecol. Environ. 5, 89–96. https://doi.org/10.1890/1540-9295(2007)5[89:HWOTRO]2.0.CO;2.

Cole, J.J., Prairie, Y.T., Caraco, N.F., et al., 2007. Plumbing the global carbon cycle: integrating inland waters into the terrestrial carbon budget. Ecosystems 10, 172–185. https://doi.org/10.1007/s10021-006-9013-8.

Cui, S., Liu, P., Guo, H., Nielsen, C.K., Pullens, J.W.M., Chen, Q., Pugliese, L., Wu, S., 2024. Wetland hydrological dynamics and methane emissions. Commun. Earth Environ. 5 (1), 470. https://doi.org/10.1038/s43247-024-01635-w.

Davidson, E.A., Kanter, D., 2014. Inventories and scenarios of nitrous oxide emissions. Environ. Res. Lett. 9 (10), 105012. https://doi.org/10.1088/1748-9326/9/10/105012.

DelSontro, T., Boutet, L., St-Pierre, A., del Giorgio, P.A., Prairie, Y.T., 2016. Methane ebullition and diffusion from northern ponds and lakes regulated by the interaction between temperature and system productivity. Limnol. Oceanogr. 61 (S1), S62–S77. https://doi.org/10.1002/lno.10335.

Dickson, A.G., 1981. An exact definition of total alkalinity and a procedure for the estimation of alkalinity and total inorganic carbon from titration data. Deep-Sea Res. I Oceanogr. Res. Pap. 28 (6), 609–623. https://doi.org/10.1016/0198-0149(81)90121-7.

dos Santos Pinto, R.M., Weigelhofer, G., Diaz-Pines, E., Brito, A.G., Zechmeister-Boltenstern, S., Hein, T., 2020. River-floodplain restoration and hydrological effects on GHG emissions: Biogeochemical dynamics in the parafluvial zone. Sci. Total Environ. 715, 136980. https://doi.org/10.1016/j.scitotenv.2020.136980.

Eschbach, D., Schmitt, L., Imfeld, G., May, J.H., Payraudeau, S., Preusser, F., Trauerstein, M., Skupinski, G., 2018. Long-term temporal trajectories to enhance restoration efficiency and sustainability on large rivers: an interdisciplinary study. Hydrol. Earth Syst. Sci. 22, 2717–2737. https://doi.org/10.5194/hess-22-2717-2018.

Forster, P., Storelvmo, T., Armour, K., et al. 2021. The Earth's Energy Budget, climate Feedbacks and climate Sensitivity. In climate Change 2021: the Physical Science Basis. Contribution of Working Group I to the Sixth Assessment Report of the IPCC [Masson-Delmotte, V., et al. (eds.)]. Cambridge University Press, Cambridge, UK, and New York, NY, USA 923–1054, doi:https://doi.org/10.1017/9781009157896.009.

Hanrahan, B.R., Tank, J.L., Dee, M.M., Trentman, M.T., Berg, E.M., McMillan, S.K., 2018. Restored floodplains enhance denitrification compared to naturalized floodplains in agricultural streams. Biogeochemistry 141 (3), 419–437. https://doi.org/10.1007/s10533-018-0431-4.

Ho, L., Barthel, M., Bodé, S., Panique-Casso, D., Six, J., Boeckx, P., Goethals, P., 2026. Bridging the gap in riverine greenhouse gas research: from monitoring methods to mechanistic understanding. J. Environ. Manag. 398, 128566. https://doi.org/10.1016/j.jenvman.2026.128566.

Holubová, K., Čomaj, M., Mravcová, K., 2016. Reconnection of the Danube floodplain channels as a vital step to restore river morphology and fluvial dynamics. In: River Sedimentation, pp. 880–887.

Hudson, P.F., Middelkoop, H., Stouthamer, E., 2008. Flood management along the lower Mississippi and Rhine Rivers (the Netherlands) and the continuum of geomorphic adjustment. Geomorphology 101 (1–2), 209–236. https://doi.org/10.1016/j.geomorph.2008. 07.001.

Kana, T.M., Darkangelo, C., Hunt, M.D., Oldham, J.B., Bennett, G.E., Cornwell, J.C., 1994. Membrane inlet mass spectrometer for rapid high-precision determination of N_2, O_2, and Ar in environmental water samples. Anal. Chem. 66 (23), 4166–4170.

Kasak, K., Kill, K., Uuemaa, E., Maddison, M., Aunap, R., Riibak, K., Okiti, I., Teemusk, A., 2022. Low water level drives high nitrous oxide emissions from treatment wetland. J. Environ. Manag. 312, 114914. https://doi.org/10.1016/j.jenvman.2022.114914.

Khoiyangbam, R.S., Chingangbam, S.S., 2022. Assessing seasonal variation of diffusive nitrous oxide emission from freshwater wetland in Keibul Lamjao National Park, Manipur Northeast India. Atmos. Environ. X 13, 100147. https://doi.org/10.1016/j.aeaoa.2022.100147.

Kim, S.Y., Veraart, A.J., Meima-Franke, M., Bodelier, P.L., 2015. Combined effects of carbon, nitrogen and phosphorus on CH_4 production and denitrification in wetland sediments. Geoderma 259, 354–361. https://doi.org/10.1016/j.geoderma.2015.03.015.

Kirschke, S., Bousquet, P., Ciais, P., et al., 2013. Three decades of global methane sources and sinks. Nat. Geosci. 6, 813–823. https://doi.org/10.1038/ngeo1955.

Knox, R.L., Wohl, E.E., Morrison, R.R., 2022. Levees don't protect, they disconnect: a critical review of how artificial levees impact floodplain functions. Sci. Total Environ. 837, 155773. https://doi.org/10.1016/j.scitotenv.2022.155773.

Koschorreck, M., Schütze, C., Ködel, U., Bussmann, I., Kamjunke, N., 2026. Phytoplankton and temperature control seasonal dynamics of greenhouse gases in a large river. J. Geophys. Res. Biogeosci. 131 (5), e2025JG009300.

Kumar, A., Medhi, K., Fagodiya, R.K., Subrahmanyam, G., Mondal, R., Raja, P., Malyan, S.K., Kumar Gupta, D., Kumar Gupta, C., Pathak, H., 2020. Molecular and ecological perspectives of nitrous oxide producing microbial communities in agro-ecosystems. Rev. Environ. Sci. Biotechnol. 19 (4), 717–750. https://doi.org/10.1007/s11157-020-09554-w.

Laini, A., Bartoli, M., Castaldi, S., Viaroli, P., Capri, E., Trevisan, M., 2011. Greenhouse gases (CO_2, CH_4 and N_2O) in lowland springs within an agricultural impacted watershed (Po River Plain, northern Italy). Chem. Ecol. 27 (2), 177–187. https://doi.org/10.1080/02757540.2010.547489.

Lang, A., Bork, H.R., Mäckel, R., Preston, N., Wunderlich, J., Dikau, R., 2003. Changes in sediment flux and storage within a fluvial system: some examples from the Rhine catchment. Hydrol. Process. 17, 3321–3334. https://doi.org/10.1002/hyp.1389.

Lauerwald, R., Allen, G.H., Deemer, B.R., et al., 2023. Inland water greenhouse gas budgets for RECCAP2: 1. State-of-the-art of global scale assessments. Glob. Biogeochem. Cycles 37, e2022GB007657. https://doi.org/10.1029/2022GB007657.

Legendre, P., Legendre, L., 1998. Numerical ecology, 2nd edition 20. https://doi.org/10.1017/CBO9781107415324.004. Dev. Environ. Model.

Leibowitz, S.G., Wigington Jr., P.J., Schofield, K.A., Alexander, L.C., Vanderhoof, M.K., Golden, H.E., 2018. Connectivity of streams and wetlands to downstream waters: an integrated systems framework. JAWRA 54, 298–322. https://doi.org/10.1111/1752-1688.12631.

Lew, S., Burandt, P., Glińska-Lewczuk, K., 2025. Microbial communities drive methane fluxes from floodplain lakes—a hydrological gradient perspective. Environ. Microbiol. 27 (6), e70127. https://doi.org/10.1111/1462-2920.70127.

Lorenzen, C.J., 1967. Determination of chlorophyll and pheo-pigments: spectrophotometric equations 1. Limnol. Oceanogr. 12 (2), 343–346. https://doi.org/10.4319/lo.1967.12.2.0343.

Lorke, A., Bodmer, P., Noss, C., et al., 2015. Technical note: drifting versus anchored flux chambers for measuring greenhouse gas emissions from running waters. Biogeosciences 12, 7013–7024. https://doi.org/10.5194/bg-12-7013-2015.

Maaß, A.L., Schüttrumpf, H., Lehmkuhl, F., 2021. Human impact on fluvial systems in Europe with special regard to today's river restorations. Environ. Sci. Eur. 33, 119. https://doi.org/10.1186/s12302-021-00561-4.

Malyan, S.K., Singh, O., Kumar, A., Anand, G., Singh, R., Singh, S., Zhiguo, Y., Kumar, J., Fagodiya, R.K., Kumar, A., 2022. Greenhouse gases trade-off from ponds: an overview of emission process and their driving factors. Water 14 (6), 970. https://doi.org/10.3390/w14060970.

McAuliffe, C., 1971. Gas chromatographic determination of solutes by multiple phase equilibrium. Chem. Technol. 1, 46–51.

Müller, B., Bryant, L.D., Matzinger, A., Wüest, A., 2012. Hypolimnetic oxygen depletion in eutrophic lakes. Environ. Sci. Technol. 46 (18), 9964–9971.

Natho, S., Venohr, M., Henshaw, A.J., 2020. Modeling the effect of enhanced lateral connectivity on river floodplain denitrification. Front. Environ. Sci. 8, 74. https://doi.org/10.3389/fenvs.2020.00074.

Newcomer Johnson, T.A., Kaushal, S.S., Mayer, P.M., Smith, R.M., Sivirichi, G.M., 2016. Nutrient retention in restored streams and rivers: a global review and synthesis. Water 8, 116. https://doi.org/10.3390/w8040116.

Oksanen, J., Blanchet, F.G., Friendly, M., et al., 2022. Vegan: Community Ecology Package. R Package Version 2.6–4.

Ollivier, Q.R., Maher, D.T., Pitfield, C., Macreadie, P.I., 2019. Winter emissions of CO_2, CH_4, and N_2O from temperate agricultural dams: Fluxes, sources, and processes. Ecosphere 10 (11), e02914. https://doi.org/10.1002/ecs2.2914.

Pander, J., Mueller, M., Geist, J., 2018. Habitat diversity and connectivity govern the conservation value of restored aquatic floodplain habitats. Biol. Conserv. 217, 1–10. https://doi.org/10.1016/j.biocon.2017.10.024.

Quick, A.M., Reeder, W.J., Farrell, T.B., Tonina, D., Feris, K.P., Benner, S.G., 2019. Nitrous oxide from streams and rivers: A review of primary biogeochemical pathways and environmental variables. Earth-Sci. Rev. 191, 224–262. https://doi.org/10.1016/j.earscirev.2019.02.021.

R Core Team, 2025. R: A Language and Environment for Statistical Computing. R Foundation for Statistical Computing, Vienna, Austria. https://www.R-project.org/.

Reckendorfer, W., Funk, A., Gschöpf, C., Hein, T., Schiemer, F., 2013. Aquatic ecosystem functions of an isolated floodplain and their implications for flood retention and management. J. Appl. Ecol. 50 (1), 119–128. https://doi.org/10.1111/1365-2664.12029.

Ribaudo, C., Benelli, S., Bolpagni, R., Darul, R., Bartoli, M., 2023. Macrophyte growth forms and hydrological connectivity affect greenhouse gas concentration in small eutrophic wetlands. Aquat. Bot. 188, 103660. https://doi.org/10.1016/j.aquabot.2023.103660.

Seitzinger, S.P., Kroeze, C., Styles, R.V., 2000. Global distribution of N_2O emissions from aquatic systems: Natural emissions and anthropogenic effects. Chemosphere Global Change Sci. 2 (3–4), 267–279. https://doi.org/10.1016/S1465-9972(00)00015-5.

Tian, H., Lu, C., Ciais, P., et al., 2016. The terrestrial biosphere as a net source of greenhouse gases to the atmosphere. Nature 531 (7593), 225–228. https://doi.org/10.1038/nature16946.

Vidon, P., Jacinthe, P.A., Liu, X., Fisher, K., Baker, M., 2014. Hydrobiogeochemical controls on riparian nutrient and greenhouse gas dynamics: 10 years post-restoration. J. Am. Water Resour. Assoc. 50 (3), 639–652. https://doi.org/10.1111/jawr.12201.

Waldron, S., Scott, E.M., Soulsby, C., 2007. Stable isotope analysis reveals lower-order river dissolved inorganic carbon pools are highly dynamic. Environ. Sci. Technol. 41 (17), 6156–6162. https://doi.org/10.1021/es0706089.

Wang, G., Xia, X., Liu, S., Zhang, L., Zhang, S., Wang, J., Xi, N., Zhang, Q., 2021. Intense methane ebullition from urban inland waters and its significant contribution to greenhouse gas emissions. Water Res. 189, 116654. https://doi.org/10.1016/j.watres.2020.116654.

Wei, T., Simko, V., Levy, M., Xie, Y., Jin, Y.J., Zemla, J., 2017. R package "corrplot". Statistician 56, 316–324. https://github.com/taiyun/corrplot.

Weiss, R., 1974. Carbon dioxide in water and seawater: the solubility of a non-ideal gas. Mar. Chem. 2 (3), 203–215.

Weiss, R.F., Price, B.A., 1980. Nitrous oxide solubility in water and seawater. Mar. Chem. 8 (4), 347–359. https://doi.org/10.1016/0304-4203(80)90024-9.

Welti, N., Bondar-Kunze, E., Tritthart, M., Pinay, G., Hein, T., 2012. Nitrogen dynamics in complex Danube River floodplain systems: effects of restoration. River Syst. 20 (1–2), 71–85. https://doi.org/10.1127/1868-5749/2011/0047.

Wickham, H., 2006. An introduction to ggplot: an implementation of the grammar of graphics in R. . Statistics 1–8.

Xiao, Q., Xu, X., Duan, H., Qi, T., Qin, B., Lee, X., Zhang, M., 2020. Eutrophic Lake Taihu as a significant CO_2 source during 2000–2015. Water Res. 170, 115331. https://doi.org/10.1016/j.watres.2019.115331.

Xiao, Q., Xu, X., Qi, T., Luo, J., Lee, X., Duan, H., 2024. Lakes shifted from a carbon dioxide source to a sink over past two decades in China. Sci. Bull. 69 (12), 1857–1861. https://doi.org/10.1016/j.scib.2024.03.022.

Zeng, L., Panizzo, V.N., Wang, Z., Huang, X., Chen, X., McGowan, S., 2025. Hydrological isolation accelerates algal blooms in floodplain lakes: Biomarker evidence from Dongting Lake, China and its satellite lake. Water Res. 279, 123430. https://doi.org/10.1016/j.watres.2025.123430.

Zhang, Y., Huang, C., Zhang, W., Chen, J., Wang, L., 2021a. The concept, approach, and future research of hydrological connectivity and its assessment at multiscales. Environ. Sci. Pollut. Res. 28 (38), 52724–52743. https://doi.org/10.1007/s11356-021-16148-8.

Zhang, W., Li, H., Pueppke, S.G., Pang, J., 2021b. Restored riverine wetlands in a headwater stream can simultaneously behave as sinks of N_2O and hotspots of CH_4 production. Environ. Pollut. 284, 117114. https://doi.org/10.1016/j.envpol.2021.117114.

Zuur, A.F., Ieno, E.N., Elphick, C.S., 2010. A protocol for data exploration to avoid common statistical problems. Methods Ecol. Evol. 1 (1), 3–14. http://www.respond2articles.com/MEE/.